

Synergistic effect of lattice, electronic and magnetic modulations on the thermoelectric behaviour of Cr-substituted $\text{La}_{0.65}\text{Bi}_{0.20}\text{Sr}_{0.15}\text{CoO}_3$

Divya Prakash Dubey ^a, M. K. Majee ^a, Rie Y. Umetsu ^b, V. Khovaylo ^c and Ratnamala Chatterjee ^{a,c*}

^a Magnetics and Advanced Ceramics Lab, Department of Physics, Indian Institute of Technology Delhi, Hauz Khas, New Delhi-110016, India

^b Institute for Materials Research, Tohoku University, 2-1-1 Katahira, Aoba-ku, Sendai 980-8577, Japan

^c National University of Science and Technology "MISiS", Leninskiy Prospect 4, 119991 Moscow, Russia

* E-mail: ratnamalac@gmail.com

Supplementary Information

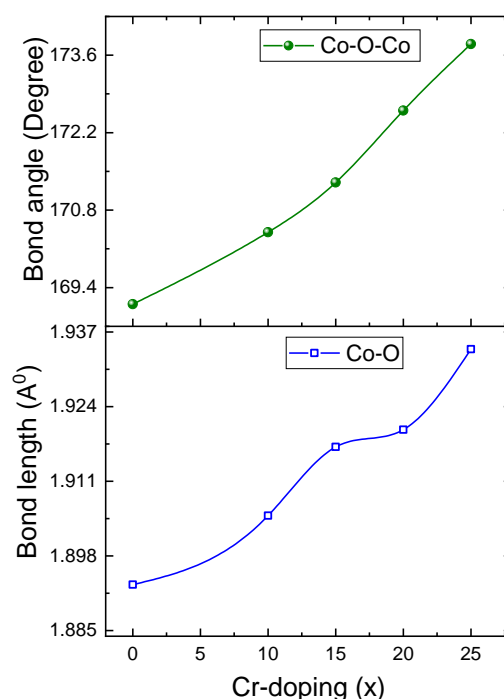


Fig. S1: Variation of Bond angle (Co-O-Co) and bond length (Co-O) with different Cr-substitution $0 \leq x \leq 25$.

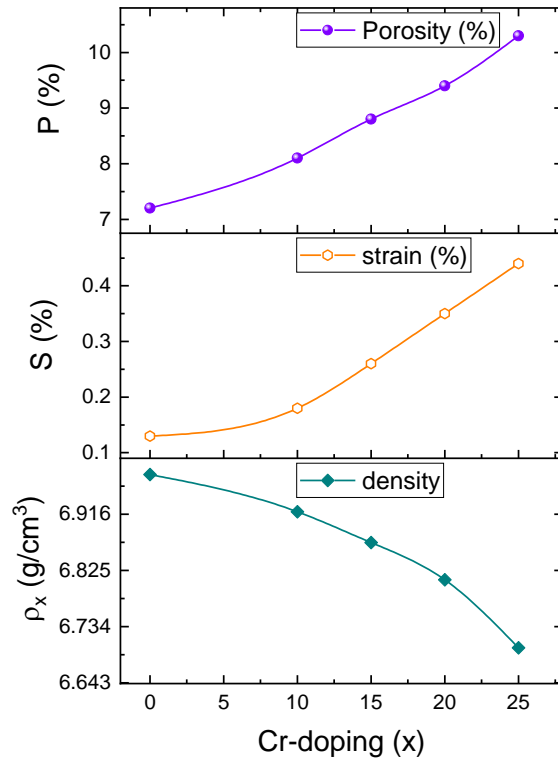


Fig. S2: Porosity, strain and x-ray density variation with different Cr-substitution $0 \leq x \leq 25$.

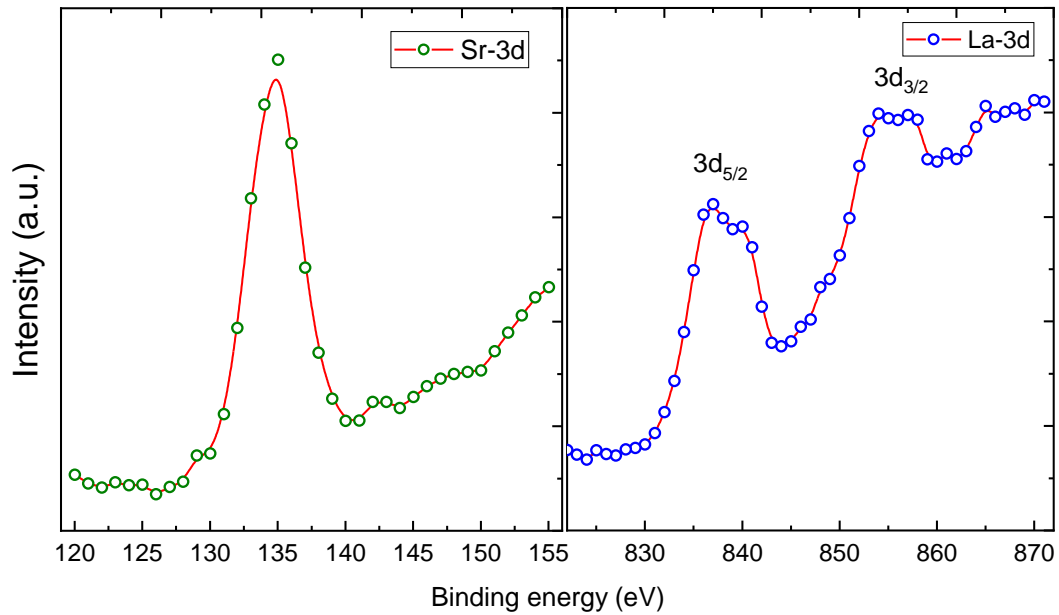


Fig. S3: Core level XPS spectra for Sr and La for Cr-25 composition.

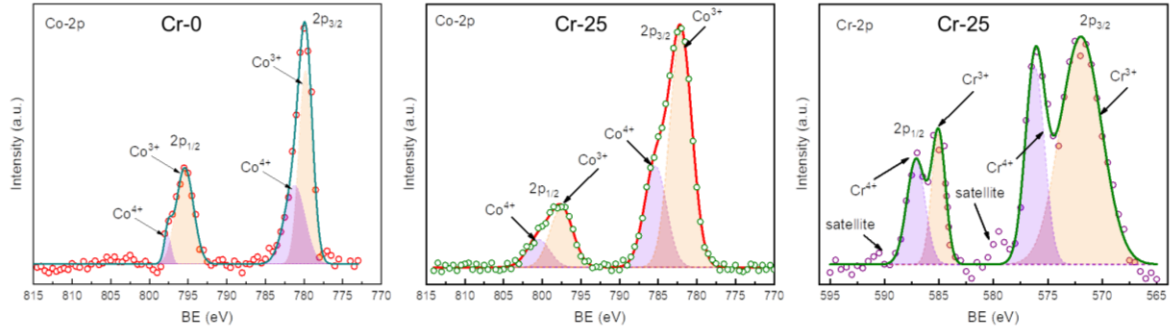


Fig. S4: Core level XPS spectra for Co-0 and Co-25, Cr-25 composition with relative peak intensity of $\text{Co}^{3+}/\text{Co}^{4+}$ and $\text{Cr}^{3+}/\text{Cr}^{4+}$ respectively.

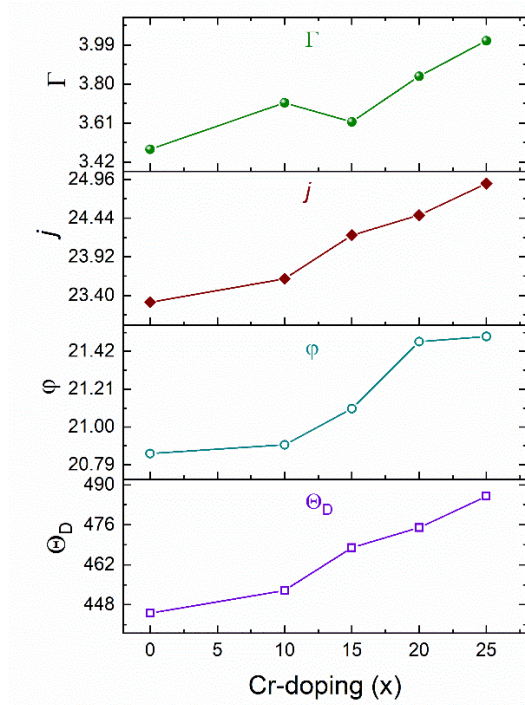


Fig. S5: Variation of electron phonon coupling strength (Γ), polaron band width (j), ϕ and debye temperature (θ_D) with different Cr-substitution i.e., Cr-0, Cr-10, Cr-15, Cr-20 and Cr-25.

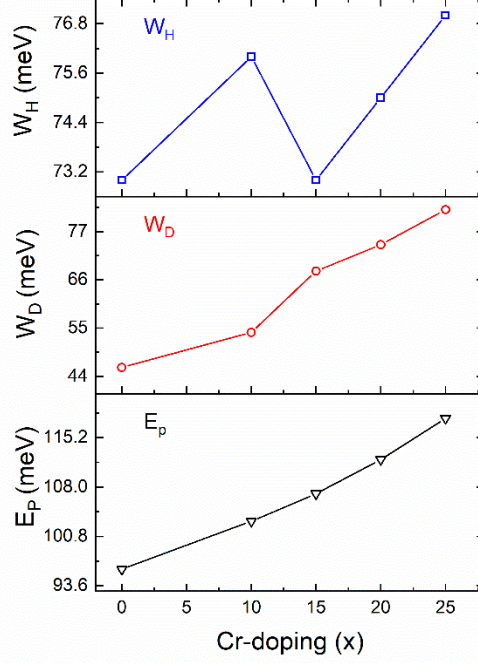


Fig. S6: Variation of W_H , W_D and E_P with Cr-substitution i.e., Cr-0, Cr-10, Cr-15, Cr-20 and Cr-25.

In-depth analysis of SPH model used for calculating the disorder energy (W_D) i.e., energy difference between two neighbouring hopping sites using the relation $E_P = W_H + (W_D)/2$, for $T > \theta_{D/2}$; however, $E_P = W_D$, for $T < \theta_{D/4}$. The calculated value of W_D lies in the range of 46-82 meV for all the compositions whereas, the hopping energy (W_H) ranging from ~70-80 meV. Using Holstein's condition, the polaron band width J ($J(T) = 0.67 \times h\nu_{ph}(T/\theta_D)^{1/4}$) and parameter ϕ ($\phi = \{(2k_B T W_H)/\pi\}^{1/4} \times \{(h\nu_{ph})/\pi\}^{1/2}$) is further calculated to confirm the energy kinetics of polaronic hopping; where, ν_{ph} is optical phonon frequency ($\nu_{ph} = k_B \theta_D/h$). The criteria for the adiabatic polaronic hopping are $J > \phi$ whereas, for non-adiabatic polaronic hopping $J < \phi$. We observed the value of $J > \phi$ for all the compositions that reflects the adiabatic nature for the hopping. The RT values of E_S , E_P , W_H , W_D , ν_{ph} , J and ϕ are tabulated in Table II of main manuscript. For all the compositions the value of $J < W_H/3$ further verified the formation of small polaron within the system. In addition, the electron-phonon ($e-ph$) coupling strength was calculated by relation $\gamma = 2W_H/h\nu_{ph}$ where, $\gamma > 4$ corresponds to strong $e-ph$ interactions. For all the compositions the large value of γ reflects the strong coupling strength for $e-ph$ interaction within the system.

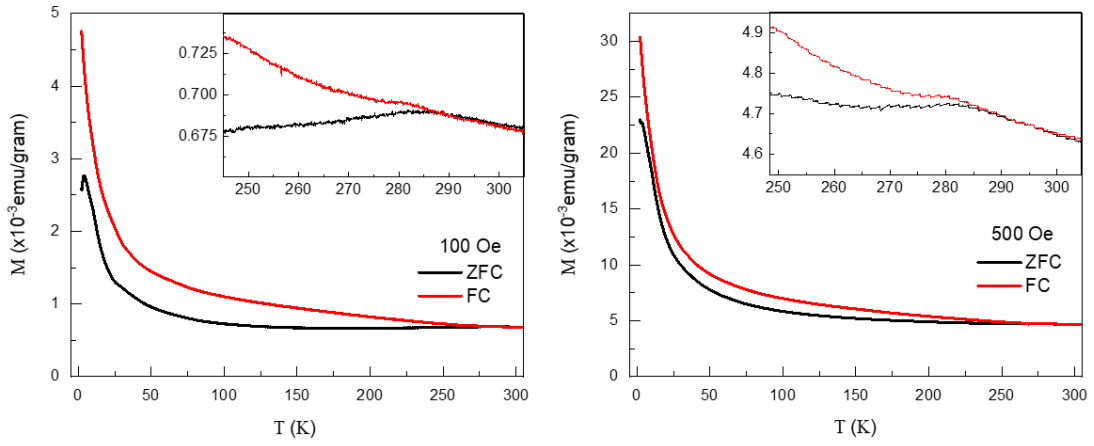


Fig. S7: Magnetization vs temperature in zero field cooled (ZFC) and field cooled (FC) geometry for Cr-25.

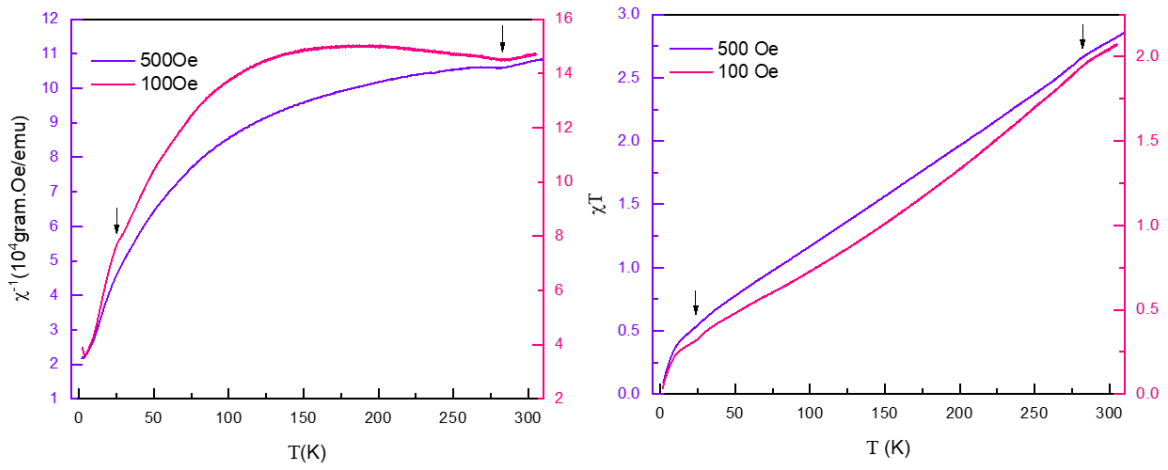


Fig. S8: Inverse susceptibility (χ^{-1}) and χT vs temperature variations for Cr-25.

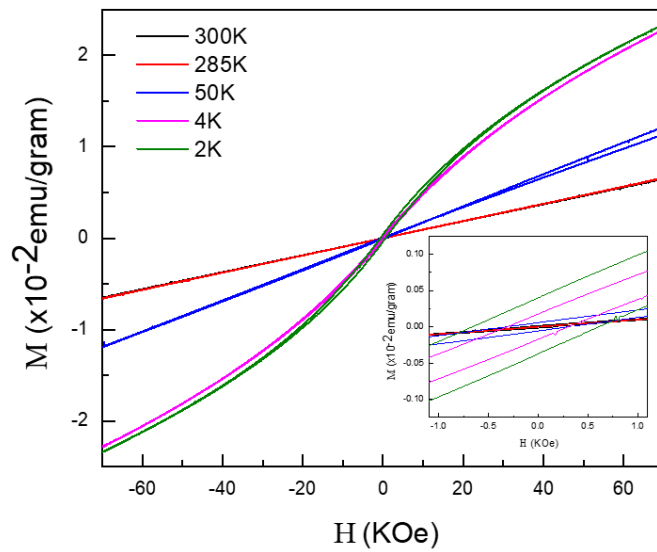


Fig. S9: Magnetization vs field variations for Cr-25 at different temperatures.

To confirm the magnetic behaviour of Cr-25, we performed the magnetization measurements with variation of temperature and magnetic field. Fig. S6 show the zero-field cooled and field cooled (ZFC-FC) measurements at 100 Oe and 500 Oe field respectively in the temperature range of $2K \leq T \leq 310K$. For both the field value the Cr-25 depicts a bifurcation at $\sim 285K$; however, comparatively large difference in ZFC and FC was observed for 100 Oe field. The large bifurcation below 285K depicts the possibility of short-range ferromagnetic ordering within the system; whereas, above this temperature a paramagnetic behaviour observed. $1/\chi$ vs T and χT vs T plots are shown in Fig. S7 for both the fields, where we observed two transitions $\sim 25K$ and $285K$. Interestingly, these transitions also appear in the specific heat (C_p) data. From the $1/\chi$ vs T plot at 100 Oe field, we observed a broad maximum $\sim 170K$ and after then a small decrease until 285K. This represents the competition between FM-AFM interactions where the AFM ordering dominates for higher temperature; however, below this temperature FM ordering overcome into the interaction. For higher field values this competitive interaction weakened that can be observed from $1/\chi$ vs T plot at 500 Oe field. This magnetic behaviour of Cr-25 compound is in good agreement with the field dependent resistivity data. The magnetization vs field (M-H) measurements at different temperature shown in Fig. S8, was performed to further clarify the magnetic state of the system. The M-H plot for 300K shows almost linear variation confirms the paramagnetic state of the system whereas at 2K there is a loop with a small value of coercivity reflects the presence of weak ferromagnetic interaction within the system. The inset of Fig. S8 shows the variation of coercivity for different temperatures. From this plot, we observed with increase in temperature the coercivity value decreases. The non-saturation of the magnetization even up to 70 kOe field depicts the canted antiferromagnetic nature that may arises due to Co^{3+} - Co^{3+} super-exchange interactions.

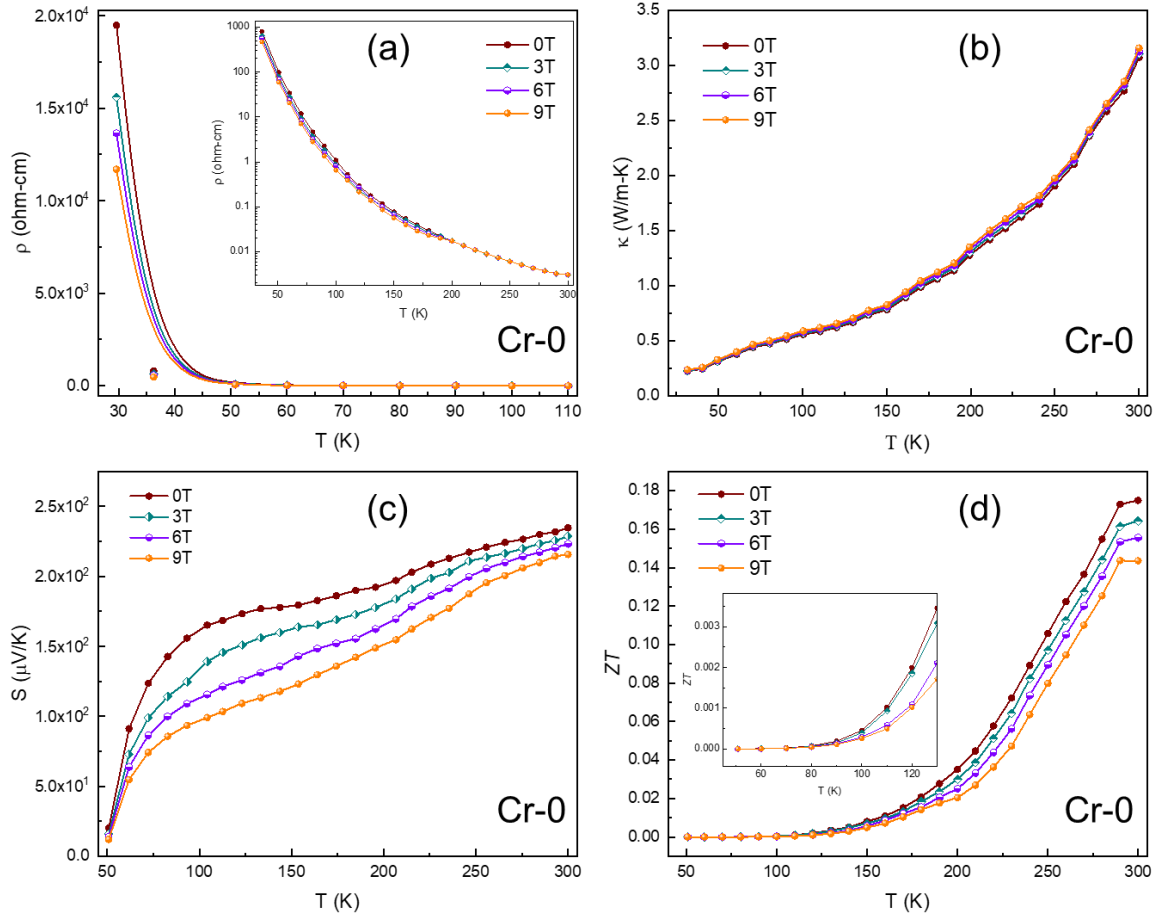


Fig. S10: Variation of resistivity, thermal conductivity, Seebeck and ZT with different magnetic field for Cr-0.

The magnetic field effect of the thermoelectric parameters of the parent compound $\text{La}_{0.65}\text{Bi}_{0.20}\text{Sr}_{0.15}\text{CoO}_3$ (Cr-0) before Cr-substitution have also been calculated. It is interesting to note that while Cr-0 at low temperature also shows negative MR of $\sim 40\%$ at $T < 50\text{K}$; Cr-25 in comparison shows $\sim 800\%$ MR in this temperature range. The magnetic field effect on Seebeck for Cr-0 depicts a small decrease in Seebeck coefficient with increasing the field at lower temperature ($T \lesssim 50\text{K}$); however, for higher temperature the field effect is almost negligible. The field dependence of thermal conductivity for Cr-0 is almost negligible and there is no significant change observed in thermal conductivity response with increasing field values. The field dependence of ZT value has also been calculated for Cr-0 composition, where we observed a monotonic decrease in ZT with increasing the field.

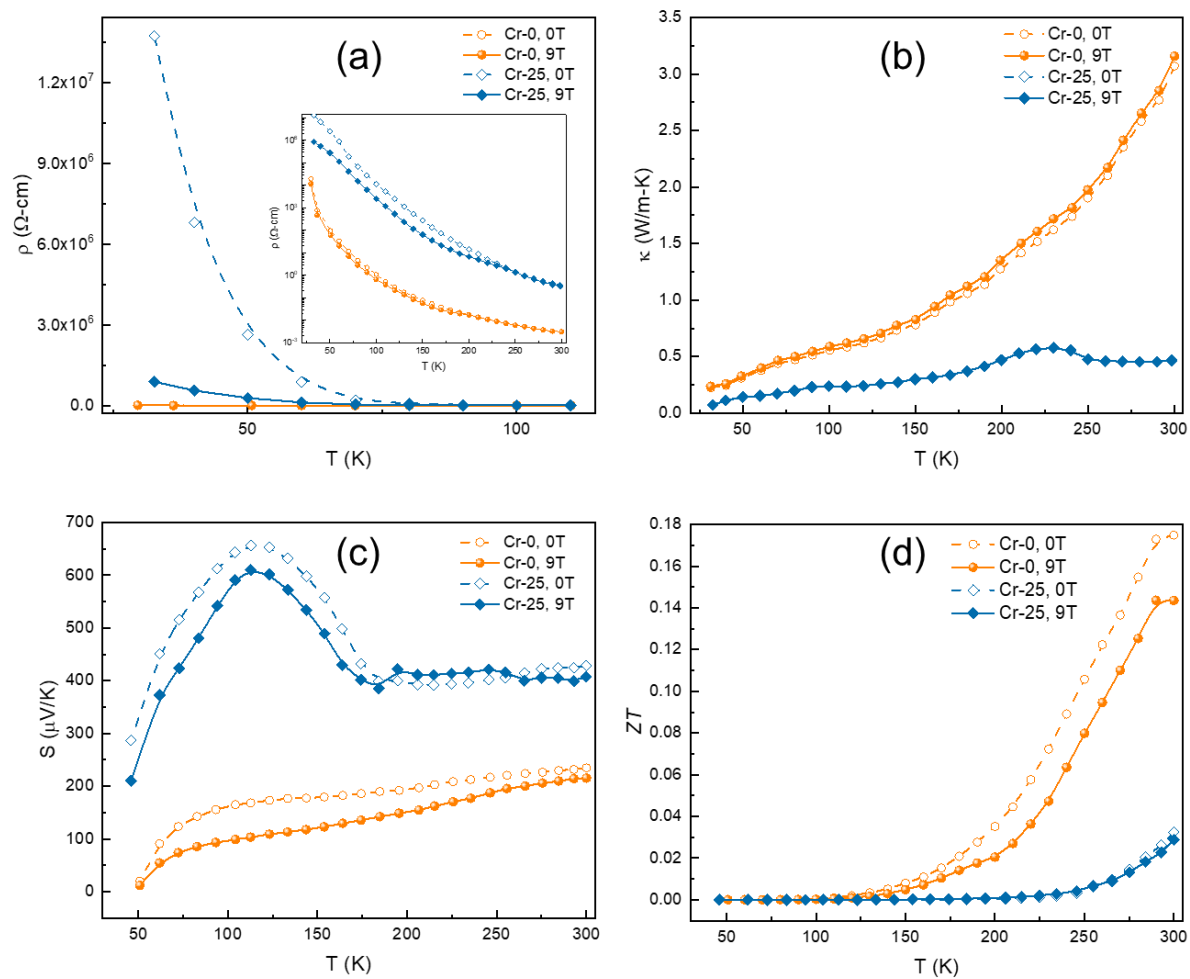


Fig. S11: Variation of resistivity, thermal conductivity, Seebeck and ZT at 0 and 9 Tesla for Cr-0 and Cr-25.

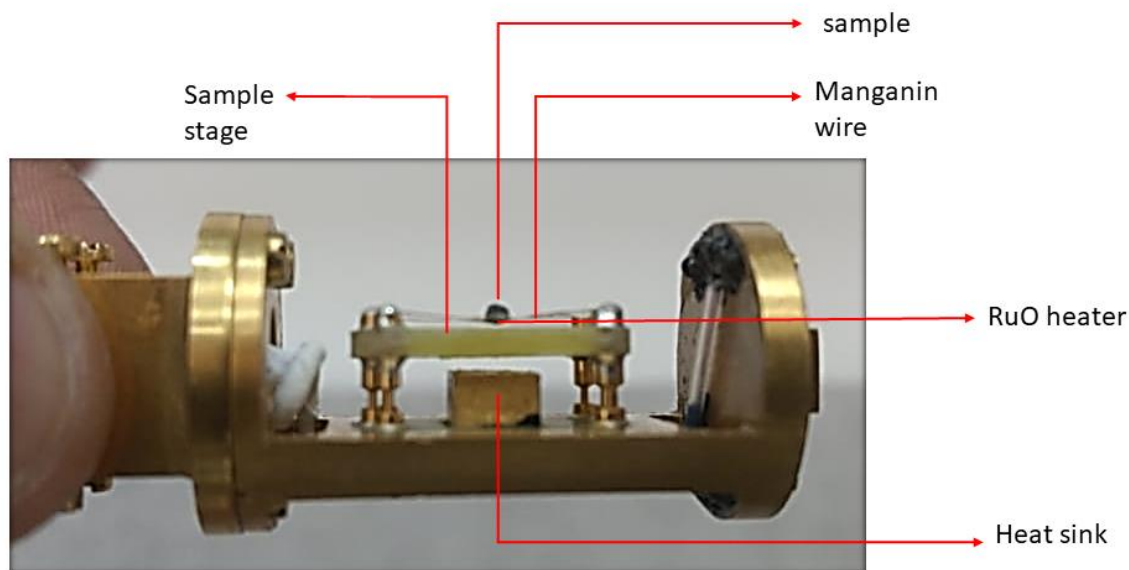


Fig. S12: Measuring setup for the heat capacity measurement where the sample is kept on RuO heater that is attached with a stage through manganin wire. The stage is in the thermal contact with bottom heat sink.

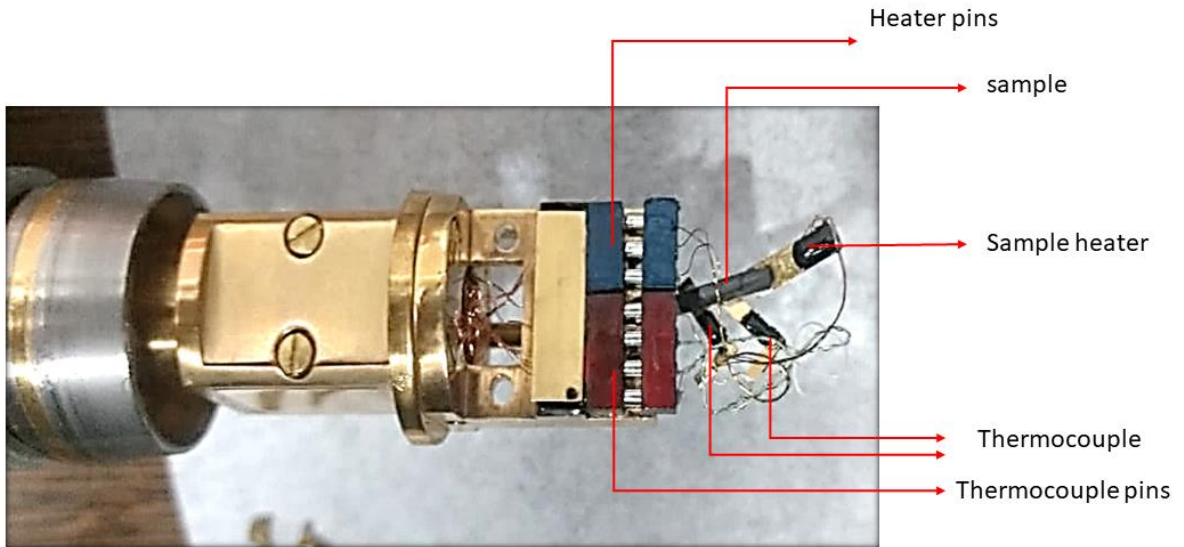


Fig. S13: Measuring setup for the Seebeck and thermal conductivity measurement where the sample is attached in between the heater and cold sink. Two k-type thermocouples attached for temperature and voltage responses.

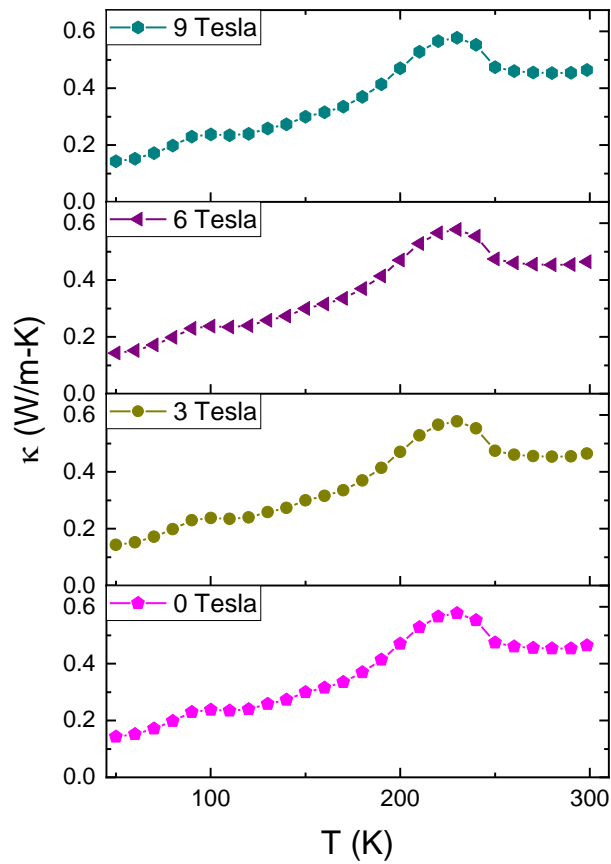


Fig. S14: Magnetic field dependent thermal conductivity variation of Cr-25.

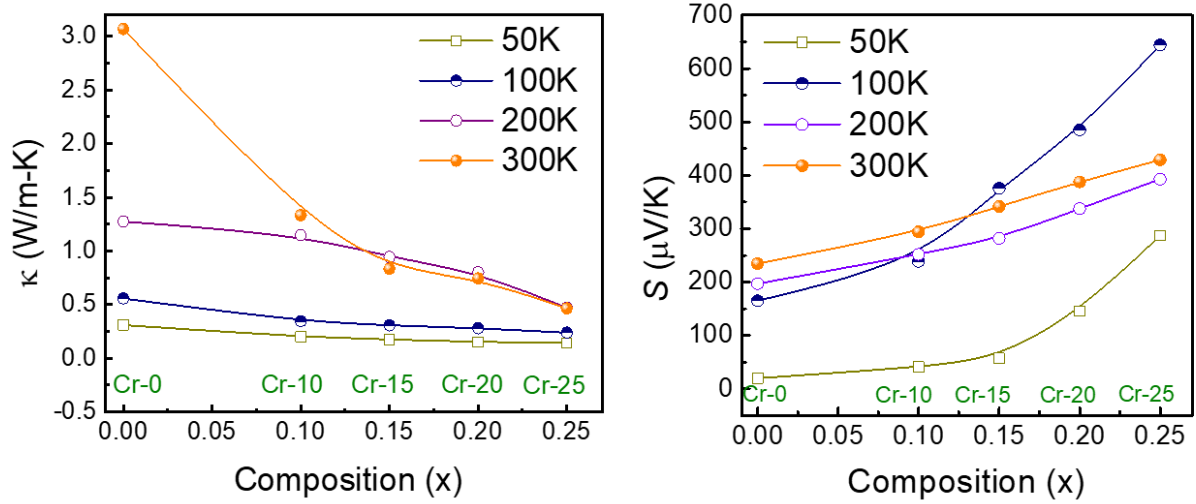


Fig. S15: Compositional variation of thermal conductivity and Seebeck coefficient with temperatures.

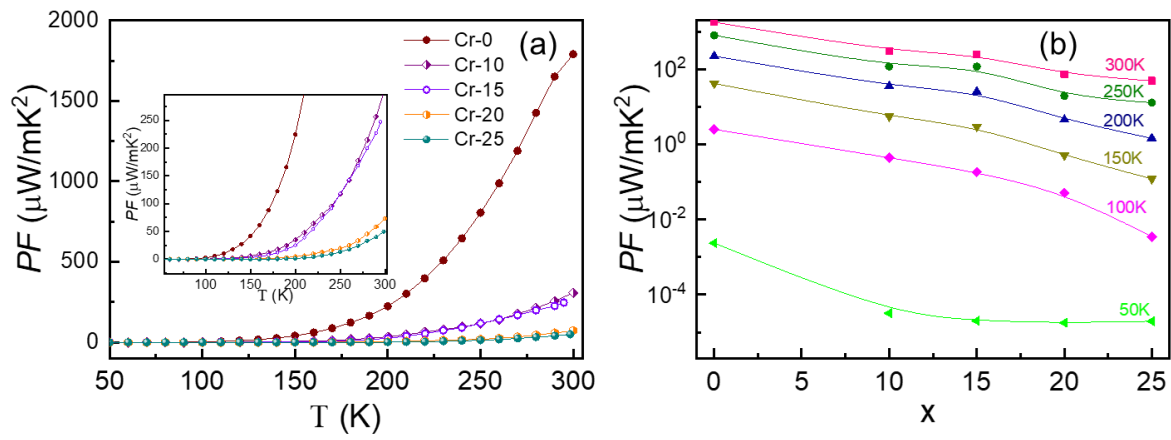


Fig. S16: Variation of power factor with Temperature (a) and composition (b) for all compositions.

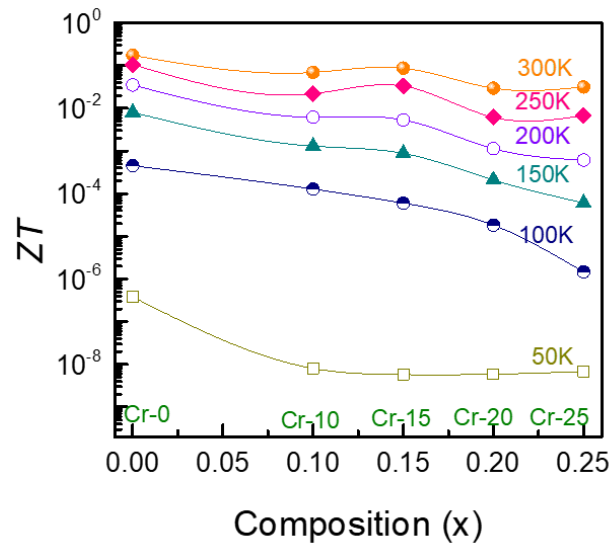


Fig. S17: Compositional variation of ZT with temperature for Cr-0, Cr-10, Cr-15, Cr-20 and Cr-25.